Links Between the Mountain Torque and the Arctic Oscillation in the LMDz General Circulation Model

F. Lott, L. Goudard, and A. Martin

Laboratoire de Météorologie Dynamique, CNRS/IPSL, Ecole Normale Supérieure, Paris, France.

F. Lott, Laboratoire de Météorologie Dynamique, Ecole Normale Supérieure, 24 rue Lhomond, 75235 PARIS Cédex 05, France. (flott@lmd.jussieu.fr)

L. Goudard, LMD/ENS Paris, (laure.goudard@ens-lyon.fr)

A. Martin, LMD/ENS Paris, (martin@lmd.ens.fr)

Abstract. Recent papers suggest that in the NCEP reanalysis data, there is a dynamical link between the mountain torque and the Arctic Oscillation (AO) at periodicities near and below 30–days. These links essentially occur because the AO is associated with a redistribution of mass from the polar regions to the midlatitudes hence giving a substantial contribution to the mass term of the Atmospheric Angular Momentum (AAM). These results are confirmed here by using a 30 years simulation done with the LMDz General Circulation Model. In particular, we verify that in the model also, the changes in mass AAM occurring during intraseasonal variations of the AO are in good part driven by the mountain torque. In this respect, the model LMDz has the great advantage to close the AAM budget near exactly, which is not the case of the NCEP reanalysis data.

As the Antarctic Oscillation (AAO) is also associated with a redistribution of mass from the polar regions to the midlatitudes, its contribution to the AAM budget is also presented. As there are much less mountains in the southern hemisphere, we show that in the model as well as in the reanalysis, the changes in mass AAM during intraseasonal variations of the AAO are in good part equilibrated by changes of opposite sign in wind AAM.

The main interest of these results is that the mountain torque drives the changes in AAM, so it can sometimes participate actively to changes of the AO, the former being associated with substantial mass AAM: the relationship is not purely passive, it has a small but significant predictive interest.

1. Introduction and motivation

During the last three decades, considerable research has been carried out on the low-frequency variability of the atmosphere. In the extratropics, Blackmon (1976), Sawyer (1976) and others have found that the variance of the 500-hPa geopotential height is larger for the low-frequency part of the spectrum, with periods longer than 10 days, than for the higher-frequency part. This low-frequency variability is essentially contained in the planetary scales and is dominated by a few spatial patterns that can be effectively extracted by Principal Components analysis (Preisendorfer 1988, Molteni et al. 1988). The leading among these patterns is the Arctic Oscillation (AO) in the Northern Hemisphere (Wallace 2000) and the Antarctic Oscillation (AAO) in the Southern Hemisphere.

Several theoretical explanations of extratropical low-frequency variability have been given. One of them follow the seminal work of Charney and DeVore (1979), who pointed out that in a low-order nonlinear quasi-geostrophic model, the interaction of the flow with large-scale topography can give rise to multiple equilibria through topographic instability. More highly resolved models (Legras and Ghil 1985; Yoden 1985) produce more complex aspects of low-frequency variability, such as periodic and aperiodic solutions, suggesting that an oscillatory form of topographic instability also exists. Other mechanisms for the extratropical low-frequency variability have been proposed, the most efficient being associated with the large-scale response to synoptic transient eddy forcing (Hoskins et al. 1983; Illari and Marshall 1983; Vautard et al. 1988).

The different theories of extratropical low frequency variability are not mutually exclusive, and at least one aspect of the theory of oscillatory topographic instability is supported

by observational evidences. Namely, mountain torques due to traveling Rossby waves affect the zonal flow in the midlatitude and affect substantially the AO. Metz (1985), for instance, has found significant cross-spectral peaks between the mountain torque (T_M) and the zonal wind at periodicities above 15 days. Lejenäs and Madden (2000) have found links between Rossby waves, mountain torque and atmospheric angular momentum (AAM) in the 6–15-day band. More recently, Lott et al. (2004) have found that changes in the AO in the 20–30-day band are preceded by a small but significant signal in the mountain torque.

The relationship between the mountain torque and the AO in Lott et al. (2004) results from the fact that the AO pattern corresponds to a redistribution of mass from the polar latitudes to the midlatitudes, hence giving a substantial contribution to the mass angular momentum term M_Ω (Lott et al. 2004). More dynamically, Lott and D'Andrea (2005) have shown that at periodicities below 25 days, the AAM response to mountain torques is equally made of mass angular momentum and wind angular momentum (M_R), the partition between the two being controlled by the geostrophic balance: when T_M is produced by mountains located in the polar regions, M_Ω is larger than M_R in the response while it is the other way round when T_M is produced by mountains located in the tropics and $M_R \approx M_\Omega$ when T_M is produced by mountains located in the midlatitudes. Consistent with these findings, and as the AO is a circulation pattern confined to the polar regions, it is natural that its relationships with T_M occurs via M_Ω rather than via M_R. These findings are supported by von-Storch (1994, 1999) who found in a coupled GCM that two among the three dominant modes of large scale variability are associated with larger M_Ω than M_R variations.

The results in Lott et al. (2004) and Lott and D'Andrea (2005) have two weaknesses. The first is that the reanalysis data are not entirely dynamically consistent: they mix analyzed products of wind and surface pressure to evaluate M_R, M_Ω, and T_M with short range forecasts of the surface friction to evaluate the boundary layer torque T_B. Even if the NCEP model was closing the AAM budget perfectly, the mixture of observations and forecasts made to produce the requested fields induces imbalances in the AAM budget. In this respect the results of Huang et al. (1999) are particularly instructive. They noted that the inclusion of the gravity wave drag to the evaluation of the total torque degrades the AAM budget closure in the NCEP data. The second weakness of the results in Lott et al. (2004) and Lott and D'Andrea (2005) is that the coherencies found between the mountain torque and the AO are in general below 0.4, even at the periodicities below 30 days where they are the largest. Although significant, these values are rather small and deserve to be cross-checked in a more dynamically consistent framework.

Furthermore, the dynamical interpretation that T_M and the AO are linked via M_Ω in Lott et al. (2004) and Lott and D'Andrea (2005) needs also to be tested by analyzing the AAM budget closure during variations of the Antarctic Oscillation. Indeed, the AAO also corresponds to a redistribution of mass from the polar latitudes to the midlatitudes and is consequently related to M_Ω variations. In this case, since there are much less mountain ranges in the Southern Hemisphere, the changes in M_Ω during the AAO must be equilibrated by other processes, like opposite changes in wind angular momentum or by the frictional torques. Again, to examine this, a dynamically consistent framework is extremely helpful.

The plan of the paper is as follows. Section 2 contains a description of the model, its midlatitude Sea-Level Pressure (SLP) variability (which includes the analysis of the model's AO and AAO), and its AAM budget. Section 3 describes the links between T_M, the AO, and the AAO. In Subsection 3.1 these links are evaluated using conventional spectral analysis techniques. In Subsection 3.2, the links between T_M and the AO are interpreted comparing composites of SLP fields keyed to intraseasonal changes in T_M and in the AO. In Subsection 3.3 composites of the AAM budget along intraseasonal changes of the AO and of the AAO are presented.

In all sections, the results from the model are compared with similar results from 30 years (1971-2000) of the NCAR/NCEP reanalysis (Kalnay et al. 1996). In some cases, the results from the reanalysis are very close from those described in Lott et al. (2004) and Lott and D'Andrea (2005) so they will be very briefly described here.

2. Model description

2.1. Variability in the model low troposphere

Our model data are derived from a 30–year simulation at 2.5^ox2.5^o horizontal resolution done with the LMDz GCM, developed at the Institute Paul and Simon Laplace. At the lower boundary, the model is forced by SSTs and Sea-Ice cover that vary along a climatological annual cycle. The model description and its winter mean climatologies are described in Lott (1999). Briefly, it has a realistic zonal mean flow and realistic steady planetary waves in the midlatitude.

Since we focus here on links between the mountain torque and the AO, it is important that the model produces a reasonable simulation of the troposphere variability. Figure 1a shows the root mean square of daily SLP variability from the model in the Northern

Hemisphere (NH) and after subtraction of the annual cycle. It reveals two major centers of action over the North-Eastern Pacific and the North-Eastern Atlantic that compare in amplitude with those from the re-analysis in Fig. 1b. In the model, these two centers of action are substantially broader than those in the reanalysis, in the sense that they extent further over the midlatitude. In particular, the model North-Eastern Atlantic Center of action is almost 10^o to the south of the corresponding center in the reanalysis. In the model, a third center of action is present near the polar region North of Siberia. It is slightly more pronounced than the corresponding one in the reanalysis (Fig. 1b).

For the Southern Hemisphere (SH) (Fig. 1c), the SLP has enhanced variance over a broad sector dubbed between the latitudes 40^oS and 20^oS and that covers half the hemisphere in longitude almost entirely to the west of the Greenwich meridian. This pattern of enhanced variance is again realistic in shape, zonal extension, and location when compared to the reanalysis in Fig. 1d. As for the NH, it nevertheless extents slightly too much toward the Equator.

The dominant patterns of atmospheric variability in the midlatitudes are captured here by projecting the sea level pressure onto the leading spatial Empirical Orthogonal Functions (EOFs, Preisendorfer 1988). We compute EOFs over both the NH and the SH, i.e. north of 30^oN and south of 30^oS respectively, again after subtraction of the annual cycle. We repeat the same analysis for the NCEP data.

The first model NH EOF (Fig. 2a) accounts for 10.5% of the SLP daily variance. It is fairly zonally symmetric and exhibits a change in sign in mid-latitudes, with one extensive and intense negative features spreading all over the Arctic and one strong positive center over the North Atlantic. It resembles to the same leading EOF in the reanalysis (Fig. 2b,

8.9% of the variance), but with three noticeable differences. The broad negative center of action covering the polar region in the EOF 1 from the reanalysis does not extent much to the south of the 50^oN latitude, while in the model it goes well beyond that over central Eurasia and the north eastern Pacific. This difference is a consequence of the fact that the center of actions for SLP variability extend too much equatorward in the model (Figs. 1a and 1b). Note also that the reanalysis EOF 1 presents a positive center over the Central North Pacific ocean that is practically absent in the model. Still in the reanalysis, the minimum over the Greenland is more pronounced than in the model.

For the SH, the first model EOF (Fig.2c) accounts for 10.9% of the SLP daily variance, and corresponds to a reinforcement of the midlatitude jet. It compares well with the AAO in the reanalysis (Fig.2d, 10.4% of the variance) in this respect. Nevertheless, it is less zonally symmetric than in the reanalysis, and it presents a ridge near the Greenwich meridian that is absent in the reanalysis.

Despite their differences from the NCEP data, the first two EOFs of the model essentially correspond to reinforced westerly jets all around the midlatitudes (as do the AO and the AAO). They also correspond to a redistribution of mass from the polar latitudes toward the midlatitudes and the subtropics, which can make them contribute to changes in mass AAM, M_Ω.

2.2. AAM budget closure

The global AAM tendency budget is given by

$$\frac{dM}{dt} = T, \tag{1}$$

where

$$M = M_R + M_\Omega, \tag{2}$$

and,

$$T = T_M + T_B + T_S. \tag{3}$$

Here M and T are the absolute atmospheric angular momentum and the total torque, while M_R, M_Ω, T_M, T_B, and T_S are the wind angular momentum, the mass angular momentum, the torque due to the mountains, the torque due to the boundary layer stress and the torque due to the subgrid-scale orographic drag (for the LMDz GCM, see Lott and Miller 1997 and Lott 1999). In the LMDz GCM, they are evaluated on-line during the model integration, every 15 minutes at each physical parameterization step. The expression for this five terms is very similar to Eqs. 5–8 given in Lott et al. (2004). After this on line evaluation, daily averages of these five quantities are formed.

Figure 3a shows the global AAM budget for the model year 1985 expressed in Hadleys (1H=10^{18} kg m^{2}s^{-2}) and from the daily series. The tendency dM/dt matches almost perfectly the total torque, the correlation between T and dM/dt being around $r = 0.98$. This is a clear advantage of using model data rather than reanalysis data: in the NCEP reanalysis the correlation between T and dM/dt is around $r = 0.87$ (Lott et al. 2004).

Figure 3b compares T_M, T_B, and T_S and shows that the mountain torque presents substantially larger fluctuations than T_B. They also occur on faster time scale. These behaviors are consistent with those in the NCEP reanalysis (Lott et al. 2004). Note as well that the torque due to the subgrid-scale orographic drag is rather small compared to both T_M and T_B. In the rest of this paper we will not discuss the role of T_S. The first

justification for this is that it is a small term that can be integrated to T_M or T_B without affecting the results. A second justification is that we wish to discuss here the torque due to the large-scale mountains, as in Lott et al. (2004) but for the NCEP data. It is also justified by the fact that in the reanalysis data, T_S degrades the AAM budget balance and is always omitted (Huang et al. 1999).

3. Links between the mountain torque and the leading modes of midlatitude variability

3.1. Spectral analysis

To evaluate at which frequencies the mountain torque, the Arctic Oscillation and the Antarctic Oscillation are related in the model, we perform here a conventional cross-spectral analysis between the corresponding series (Fig. 4, see caption for details on the method). For the AO index and for the AAO index, we use the leading principal components (PC 1) issued from the EOFs analysis in Section 2.1. The black line in the top panel of Fig. 4a presents the coherency between the mountain torque series and the AO index. It is above 0.25 and significant for near all periodicities below 50 days ($\omega > 0.02$cy/day), it is near to 0.4 for periodicities below 20 days, approaching 0.5 at the end of the spectra (for $\omega > 0.2$cy/day). The phase (black line in the lower panel of Fig. 4a) remains around $-\pi/2$, at least for all values of the frequency ω for which the coherency is significant. By contrast, the coherency between the mountain torque and the AAO index (grey line in the top panel of Fig. 4a) is nearly never significant. It only approaches the 1% confidence levels for rather long periodicities, i.e. when $\omega < 0.02$cy/day.

The same analysis for the NCEP data in Fig. 4b shows that the spectral relationships between the mountain torque, the AO and the AAO in the model are representative of

those in the re-analysis. Note however, that in the NCEP data, the coherency between T_M and the AO index only becomes significant at periodicities below 33 days.

The same cross spectral analysis have been carried out between the mass angular momentum M_Ω, the AO, and the AAO (not shown). At nearly all frequencies in the model and in the reanalysis, M_Ω is in phase with the PC 1s series. In general the coherencies are between 0.3 and 0.6 at all periodicities, and always significant (for the NCEP data and the AO, see for instance the Fig. 2d in Lott and D'Andrea 2005).

3.2. Composite analysis of sea-level pressure fields

To explain the lead-lag relationships between the T_M and the AO in Fig. 4 we can make 4 non-exclusive hypothesis. In two of them, T_M precedes the AO. In these cases when T_M is positive (negative) it accelerates (decelerates) the zonal flow in the midlatitudes a process that can lead to increase (decrease) the AO signal at a latter stage. In the other two hypothesis T_M follows the AO. and in these cases when the AO signal is positive (negative) it can return to a smaller (larger) value under the action of a positive (negative) T_M. To address which among these hypothesis is relevant for the surface climate, we have made a composite analysis of the sea-level pressure maps keyed to the series of the mountain torque T_M and of the AO.

To increase the statistical significance of our results we next focus onto the intraseasonal (IS) 10–150-day band. Although this band is rather large and often used in the literature (Ghil and Mo 1991), this choice implies that we exclude from the composite analysis the interannual variability. This is justified by the fact that at long periodicities the boundary layer torque dominates the mountain torque substantially (Rosen 1993). We also exclude the synoptic variability which is dominated by the baroclinic eddies. This is justified by

the fact that this variability is not well captured by the AO. Note also that the results in Lott et al. (2004) concern the 20–30-day band, and that the coherences in Fig. 4a are only significant for periodicities below 50-day. These bounds guarantee that the IS-band captures a large part of the relationships between the mountain torque and the AO we discuss here.

To focus onto the IS-band, we follow Ghil and Mo (1991) and first apply to all series and maps the high-pass filter due to Papoulis (1993) which is defined by the minimum bias taper,

$$W_0(t) = \frac{1}{\pi}\left|\sin\frac{\pi t}{L}\right| + \left(1 - \frac{|t|}{L}\right)\cos\frac{\pi t}{L},\ \text{for } |t| < L;\ W_0(t) = 0,\ \text{for } |t| > L. \qquad (4)$$

A choice of maximum lag $L = 90$ gives the half-power point of the frequency window associated with $W_0(t)$ at 150 days. To filter out the synoptic transient eddies we next apply the low-pass filter developed by Blackmon and Lau (1980), whose half-power point is around 10 days. The resulting series are referred to as the IS series.

Figures 5a–c show the model composites of sea level pressure that are associated with negative values of the IS T_M. These composites are built from IS SLP maps selected when the IS T_M presents a local extrema which amplitude is larger than a threshold value equal to 2.3 time the standard deviation of the IS T_M series ($\sigma(T_M)$). At zero lag for instance (Figure 5b), the composite is the average of the IS SLP maps over the N^+ dates when the IS T_M has a local minimum that is smaller than $-2.3\,\sigma(T_M)$, minus the average of the IS SLP maps over the N^- dates when the IS T_M has a local maximum that is larger than $+2.3\,\sigma(T_M)$. The total number N of extrema in T_M selected in Fig 5 is $N = N^+ + N^-$=85, with $N^+ = 50$ and $N^- = 35$. At a given nonzero lag, the composites are built with those maps that each correspond to a date situated at the given lag from

the local extrema identified before in the IS T_M. The threshold value of $2.3\,\sigma(T_M)$ taken here is rather arbitrary, it ensures that between two and three dates are selected each year to build the composites. Note that we verified that the results are not much sensitive to moderate changes in this threshold. Areas that equal or exceeds a 1% student test for the significance are shaded.

The choice to key our composites to minus the IS T_M rather than to the IS T_M is a complication that deserves some comments. In the model, it happens that there is a rather pronounced asymmetry between negative and positive extrema in the mountain torque, with substantially more minima then maxima (see Fig. 3b). Predominantly, the model IS T_M becomes large and negative to decelerate the flow. We could have contrasted composite maps where the IS T_M is negative and maps where it is positive and discussed the difference. For brievity, and because we did not observe such a difference in the reanalysis data, we do not do it here. To summarize, the composite patterns in Fig 5 essentially results from negative values of the IS T_M, hence our choice here to key our composites to negative values in the corresponding series.

At zero lag with respect to the extrema of T_M (Fig 5b), the composite essentially shows east-west dipoles over the Rockies and the Himalayas respectively. Over both mountain massifs, the composite pattern is positive to the west and negative to the East. According to this composite map, a negative IS T_M is due to the zonal pressure differences over these two major massifs.

The flow deceleration associated with negative IS torque in the model, is clearly substantial and significant before and after the extrema selected. At -5 day lag (Fig 5a) the flow in the NH is predominantly anticyclonic over near the whole polar region, while it

is predominantly cyclonic at +5 day lag (Fig 5c). If we now compare the flow pattern in Fig 5a with the AO pattern in Fig. 2a, there is a clear positive correlation. Conversely, the flow pattern in Fig 5c correlates with minus the AO pattern in Fig. 2a. This result suggests that changes in the AO can be produced by the mountain torque, at least in part and from time to time.

If this is true, the composites according to the IS AO must show patterns, at non-zero lag, that correlate well with the SLP pattern associated with a substantial torque in Fig 5b. This point is checked in Fig 6 which shows composites keyed to minus the IS-AO. As for the composites keyed to the IS-T_M the maps selected correspond to days where the IS-AO presents extrema that exceed 2.3 times the standard deviation of that series, yielding $N^+ = 40$ and $N^- = 42$. Before a negative extrema in the IS AO (Fig. 6a) the sea-level pressure clearly presents negative zonal gradients over the Rockies and the Himalayas that can lead to a negative torque. More precisely, over the Rockies, this negative gradient is due to the high SLP pattern that is centered over northern eastern Pacific, slightly to the south of the Alaskan peninsula in Fig. 6a. The negative pressure gradient over the Himalayas is due to the low SLP pattern that is centered over eastern Asia in Fig. 6a. The same patterns are clearly present in the composite that gives a large negative mountain torque in Fig 5b. Note also that after an negative extrema in the IS-AO (Fig. 6c) the SLP composite does not present clear zonal pressure gradients over the Rockies and the Himalayas. The mountain torque signal is presumably larger before the Ao than after.

We have also made the composite maps in Fig 5 and Fig 6 using the NCEP data (not shown). The results are very similar to those in Fig. 5 and 9 in Lott et al. (2004) so we

will not repeat their description here. The overall behaviour of the model is comparable with that of the reanalysis, at least concerning the composites keyed to the IS mountain torque (compare Fig. 5b here with minus Fig. 5a in Lott et al. 2004, and Fig. 5c here with minus Fig. 5b in Lott et al. 2004). For those keyed to the IS-AO the fact that they can give rise to a mountain torque at non-zero lag is clearer in the reanalysis data than in the model (not shown but compare for instance the Fig 6a with the Fig. 9b in Lott et al. 2004). In particular, in the NCEP data, the dipole structures in sea-level pressure over the Rockies and the Himalayas that lead to a large negative torque are also clearly apparent in the composites keyed to minus the IS AO and at -5 day lag (not shown). Still in the NCEP data, the SLP composite 5-day after a large negative IS AO resemble to that associated with a positive IS torque at O-day lag (not shown again but see Fig. 9b in Lott et al. 2004). In the reanalysis data, it seems that a signal on the mountain torque can equally precede and follow the AO, while in the model it seems more pronounced before the AO.

3.3. Composite analysis of the AAM budget

To establish more quantitatively that the mountain torque can sometime drive change in the AO, it is essential to notice that the AO pattern in Fig. 2a corresponds to a redistribution of mass from the polar regions toward the mid-latitudes and the tropics. It is thus associated with modifications in mass angular momentum which characteristic amplitude can be estimated by taking for the surface pressure in the estimation of M_Ω (Eq. 6 in Lott et al. (2004)) the EOF pattern in Fig. 2a. Then, multiplying the value obtained by the standard deviation of the PC-1, a characteristic value near 30Hd is obtained. As the standard deviation of M_Ω is around 70Hd, and as the changes in M_Ω are in good part

driven by the mountain torque, it is clear that the mountain torque is large enough to move the AO back and forth.

To support this more precisely, Fig. 7a presents the evolution of the IS composites of different terms in the AAM budget keyed to minus the IS AO (the days selected are those used for the SLP composites in Fig. 6). These composites are compared to composites of the AAM budget keyed to minus the IS-AO in the NCEP data (Fig. 7b, threshold equals to 2.3 times the standard deviation of the IS-AO, yielding $N = 83$). In the composites from the model (Fig. 7a), the mountain torque (T_M thick black) has a large and negative value below -15H at -5 day lag. It becomes positive and near 10H at +5 day lag. It follows well the composites of the total torque (T thick black dashed) witnessing that the mountain torque is the major contributor to the AAM variations when the IS-AO varies. It is important to note here that the mass AAM tendency (dM_Ω/dt thick grey) follows well the total AAM tendency (dM/dt thin grey). Both curves are very near to each other at positive lag and differ by less then 5Hd at negative lag, a value that is marginally significant at the 1% confidence level. To summarize, when the AO varies in the model, the mass AAM varies as well and the variations in mass AAM are essentially driven by the mountain torque.

The fact that the model data support the results obtained from the reanalysis data is well illustrated comparing Fig. 7a and Fig. 7b. Overall, the model behaves in agreement with the observations, giving an independent and dynamically consistent confirmation that the mountain torque can affect the AO via the mass angular momentum. This confirmation was needed because in the NCEP data the composite of the AAM budget

is not closed as well as it is the LMDz GCM: the total torque and the AAM tendency match very well in Fig. 7a, they do not in Fig. 7b.

As said in the introduction, another approach to evaluate the significance of the mountain torque onto the AO dynamics is to compare AAM budgets composites during variations of the IS-AO and of the IS-AAO. For the model IS-AAO, this is done in Fig. 8a, where the composites are built selecting $N = 85$ dates where the IS-AAO presents extrema that exceed 2.1 times its standard deviation. The thick grey line in Fig. 8a shows that the mass AAM decreases before the IS-AAO reaches a minimum ($dM_\Omega/dt < 0$ at negative lag) and increases after this minimum ($dM_\Omega/dt > 0$ at positive lag). These tendencies in M_Ω are associated with comparable tendencies in total angular momentum M, but the amplitudes of the extrema in dM/dt (thin grey line) are less pronounced than those in dM_Ω/dt. The extrema in dM/dt also present a delay of 2 to 3 days compared to those in dM_Ω/dt. These differences in amplitude and phase have two origins. First, a substantial fraction of the dM_Ω/dt variations are equilibrated by variations of opposite sign in dM_R/dt (thick grey dashed in Fig. 8a). Second, the torques (T_M and T, thick black solid and thick black dashed respectively) peak at rather small negative lag. In this circumstance it is much more difficult than for the AO to say that the mountain torque T_M drives the changes in M_Ω because the M_Ω tendency and the mountain torque are closer to being in quadrature than in phase.

It is again important to note that the behaviour of the AAM budget during IS-variations of the model AAO, represents well that in the NCEP reanalysis (Fig. 8b, same value for the threshold as in Fig. 8a, yielding $N = 82$). Also in the reanalysis, the changes in mass AAM occurring during variations of the AAO (dM_Ω/dt thick grey) are in good part

equilibrated by changes of opposite sign in wind AAM (dM_R/dt thick grey dashed), with the torques being more passive than for the AO. Nevertheless, in the composites from the reanalysis (Fig. 8b), there are large errors between dM/dt (thin grey line) and T (thick black dashed). Hence, the fact that the changes in mass AAM are in good part equilibrated by changes of opposite sign in M_R is much more difficult to assess. The fact that this balance occurs without ambiguity in the model helps to conclude that this equilibration is likely to occur in reality as well.

4. Conclusion

A 30-year integration done with the tropospheric version of the atmospheric GCM LMDz has been used to analyze the links between the mountain torques and the Arctic Oscillation. The model results have been systematically compared with those from the NCEP reanalysis, and which have been extensively discussed elsewhere (Lott et al. 2001, 2004; Lott and D'Andrea 2005). To control that the LMDz model is adapted for this purpose, we have first verified that it has a reasonable intraseasonal variability in sea-level pressure fields (Fig. 1). In particular, its leading modes of variability in the NH and in the SH are reminiscent of the Arctic Oscillation and of the Antarctic Oscillation respectively (Fig. 2). Second, we have verified that the model closes perfectly the AAM budget (Fig. 3a).

To detect possible links between the mountain forcing and the AO, we have first proceeded to a cross-spectral analysis between the mountain torque and the first component of NH sea-level pressure variability (Fig. 4a). In the model, the mountain torque and the AO present significant coherencies at periodicities below 50-days, i.e over a substantially larger band than in the reanalysis (Fig.4b). The fact that the mountain torque can affect

the AO evolution follows that the mountain torque and the AO index are in lead-lag relationship, with the torque leading in near quadrature. It can either mean that positive (negative) values of T_M have a tendency to precede positive (negative) values of the AO or/and that negative (positive) values of the T_M have a tendency to follow positive (negative) values of the AO.

To precise which signal follows the other, and which sign of the mountain torque is predominant, we have proceeded in Section 3 to several composite analysis. As the AO is a pattern of low-frequency variability, and as the cross-spectral analysis only shows significant relationships at periodicities below 50 days in the model and below 30 days in the reanalysis, we have limited the composite analysis to the conventional 10–150-day intraseasonal band (Ghil and Mo 1991).

The composites of SLP maps in Figs. 5 and 6 reveal several important results. First, the extrema in IS-mountain torque are associated with SLP dipoles across the Rockies and the Himalayas which are rather substantial in amplitude (around 10hPa from minima to maxima) and significant at the 1%-level (Fig. 5b). These dipoles are comparable with those from the reanalysis (see Fig. 5a in Lott et al. 2004) witnessing that comparable mechanisms produce the mountain torque in the model and in the reanalysis. Second, the mountain torque induces circulation changes that are rather substantial and significant in the NH. In large zones, North of 30^ON, the circulation is predominantly cyclonic before a negative torque (Fig. 5a), and anticyclonic after (Fig. 5c). Again this is consistent with what occurs in the reanalysis data. Note nevertheless that in the model, there is an asymmetry between negative and positive mountain torque anomalies, the former being

often larger in amplitude than the latter. Accordingly, the patterns in Figs. 5a and 5b essentially result from flow decelerations associated with negative mountain torques.

The composites of SLP maps in Fig. 6 show that the negative IS-AO anomalies in the model are preceded by a SLP pattern that can lead to a substantial negative mountain torque (Fig. 6a), while at positive lag, the relationship with the mountain torque is less clear (Fig. 6c). In the model, it is thus essentially negative phases of the AO that have a negative IS mountain torque precursor.

The fact that the model AO can be moved back and forth by the mountain torque is established more quantitatively by two other pieces of evidence. First we measure the "inertia" of the AO, by calculating the mass AAM that corresponds to the EOF 1 pattern in Fig. 2a. When we multiply this value by the AO-index standard deviation, the value obtained is comparable in magnitude but substantially smaller than the standard deviation of M_Ω. If the variations in M_Ω are driven by the mountain torque, then the mountain torque is large enough to affect the AO substantially.

The composites of the AAM budget keyed to minus the IS-AAO in Fig. 7a confirm this last hypothesis. It shows that M_Ω decreases before a minima in the IS-AO and increases after. These variations are near those in total AAM M, the tendencies of the wind term M_R being small (which was dynamically explained in Lott and D'Andrea 2005) and are almost entirely due to the mountain torque (the boundary layer torque being small). Note here that the positive signal in the IS mountain torque after the negative IS-AO is smaller than the negative torque signal before, consistently with the results in Fig 6. Except for this last point, all these results are also consistent with those found in the reanalysis (Fig. 7b).

Despite some qualitative differences, the model thus confirms the results in Lott et al. (2004) and Lott and D'Andrea (2005) which link the mountain torque and the Arctic Oscillation via the mass angular momentum term.

It is interesting to note that the Southern Hemisphere provides a null hypothesis for these findings. Indeed, the variability in the SH is also dominated by an annular mode, the AAO, that corresponds to a redistribution of mass from the polar regions to the midlatitudes and subtropics. Hence, variations in the AAO also result in variations in mass AAM. Nevertheless, as there are much less mountain ranges in the SH, those variations can not be related to the mountain torque as well as in the NH. This point has been extensively verified all along the paper, in the model, as well as in the reanalysis.

First, the spectral coherency between the mountain torque and the AAO are almost never significant (Fig. 4), while the spectral coherency between M_Ω and the AAO is near always significant. Second, the mass AAM variations that occur when the IS-AAO varies are in good part equilibrated by variations of opposite sign in wind AAM (for the model and the reanalysis, see Fig. 8).

The results presented here confirm that the mountain torque plays an active role in the NH intraseasonal variability. Since the mountain torque produces significant changes in the AO, it can have a predictive value. Nevertheless, the mountain torque is only one among the many other dynamical processes that affect the AO and its predictive value still remains to be evaluated. The results of this paper show that General Circulation Models can be used for this purpose.

Although we have only shortly discussed the significance of the Subgrid Scale Orography parameterization in the AAM budget, its small impact was rather disappointing. Indeed

the Lott and Miller (1997) scheme used here is rather efficient in improving the LMDz NH climatology (Lott 1999), at least concerning the steady planetary waves and the zonal mean winds. It seems here that global AAM-budget studies are of little help to tune such schemes. This is rather unfortunate because there are no global datasets that document the small-scale mountains drag all around the globe: it would have been useful to find a substantial relationships between the SSO torque and the AAM, because the AAM affects the length of the day that is measured routinely. Nevertheless, in this work, we did not carry out sensitivity tests of the global AAM budget to changes in the parameters of Lott and Miller (1997) scheme. They may have an indirect impact on the mountain torque for instance, that still remains to be evaluated.

Acknowledgments. We thank Fabio D'Andrea for helpful discussions, and who also carefully read the paper.

References

Blackmon, M. L. (1976), A climatological study of the 500 mb geopotential height of the northern hemisphere, *J. Atmos. Sci.*, *33*, 1607–1623.

Blackmon, M. L., and N. C. Lao (1980), Regional characteristics of the Northern Hemisphere wintertime circulation: A comparison of the simulation of the GFDL general circulation model with observations, *J. Atmos. Sci.*, *37*, 497–514.

Charney, J., and J. G. DeVore (1979), Multiple flow equilibria in the atmosphere and blocking, *J. Atmos. Sci.*, *36*, 1205–1216.

Hoskins, B. J., I. N. James, and G. H. White (1983), The shape, propagation and mean-flow interaction of large-scale weather systems, *J. Atmos. Sci.*, *40*, 1595–1612.

Huang, H. P., P. D. Sardeshmuk, and K. M. Weickmann (1999), The balance of global angular momentum in a long-term atmospheric data set. *J. Geophys. Res.*, *104*, D2, 2031–2040.

Ghil, M., and K. Mo (1991), Intraseasonal oscillations in the global atmosphere. Part I: Northern Hemisphere and tropics. *J. Atmos. Sci.*, *48,* 752-779.

Illari, L., and J. C. Marshall (1983), On the interpretation of eddy fluxes during a blocking episode, *J. Atmos. Sci.*, *40*, 2232–2242.

Legras, B., and M. Ghil (1985), Persistent anomalies, blocking and variations in atmospheric predictability, *J. Atmos. Sci.*, *42*, 433–471.

Lejenäs, H., and R. A. Madden (2000), Mountain torques caused by normal-mode global Rossby waves, and the impact on atmospheric angular momentum, *J. Atmos. Sci.*, *57*, 1045–1051.

Lott, F., and M. Miller (1997), A new subgrid scale orographic drag parameterization; its testing in the ECMWF model, *Quarterly Journal of the Royal Meteorological Society*, *123*, 101–127.

Lott, F. (1999), Alleviation of stationary biases in a GCM through a mountain drag parametrization scheme and a simple representation of mountain lift forces, *Monthly Weather Review*, *127*, 788–801.

Lott, F., A. W. Robertson and M. Ghil (2001), Mountain torques and atmospheric oscillations, *Geophys. Res. Lett.*, *28*, 1207-1210.

Lott, F., A. W. Robertson, and M. Ghil (2004), Mountain torques and Northern-Hemisphere low-frequency variability Part I: Hemispheric aspects, *J. Atmos. Sci.*, *61*, 1259–1271.

Lott, F. and F. D'Andrea (2005), Mass and wind axial angular momentum responses to mountain torques in the 1–25 day band. Links with the Arctic Oscillation, *Quart. J. Roy. Meteor. Soc.*, *In Press*.

Metz, W. (1985), Wintertime blocking and mountain forcing of the zonally averaged flow: a cross-spectral time series analysis of observed data, *J. Atmos. Sci.*, *42*, 1880–1892.

Molteni, F., S. Tibaldi, and T. Palmer (1990), Regimes in the wintertime circulation over northern extratropics. Part I: observational evidence, *J. Atmos. Sci.*, *47*, 31–67.

Papoulis, A. (1973), Minimum bias windows for high resolution spectral estimates, *IEE Trans. Info. Theory*, *19*, 9–12.

Preisendorfer, R. W. (1988), Principal Component Analysis in Meteorology and Oceanography, *Elsevier, Science*, New-York, 425 pp.

Rosen, R. D. (1993), The axial momentum balance of Earth and its fluid envelope, *Surv. Geophys.*, *14*, 1–29.

Sawyer, J. S. (1976), Observational characteristics of atmospheric fluctuations with a time scale of a month, *Q. J. Roy. Meteorol. Soc.*, *96*, 610–625.

Vautard, R., B. Legras, and M. Déqué (1988), On the source of midlatitude low-frequency variability. Part I:a statistical approach to persistence, *J. Atmos. Sci.*, *45*, 2811–2843.

Yoden, S. (1985), Multiple stable states of quasi-geostrophic barotropic flow over sinusoidal topography, *J. Meteor. Soc. Japan*, *63*, 1031–1045.

von Storch, J.-S. (1994), Interdecadal variability in a global coupled model, *Tellus*, *46a*, 419–432.

von Storch, J.-S. (1999), The reddest atmospheric modes and the forcing of the spectra of these modes, *J. Atmos. Sci.*, *56*, 1614–1626.

Wallace, J. M. (2000), North Atlantic Oscillation/annular mode: Two paradigms - one phenomenon, *Quart. J. Roy. Meteor. Soc.*, *126*, 791–806.

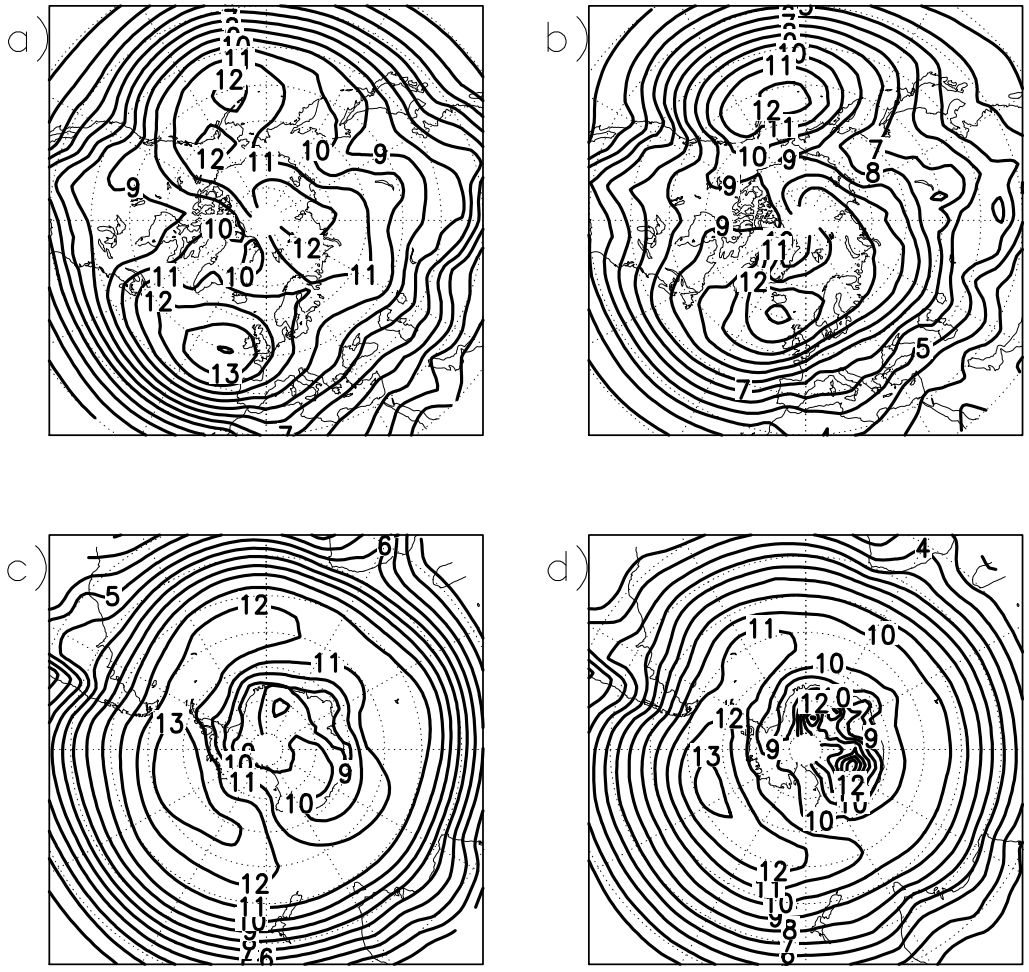

Figure 1. Standard deviation of sea-level pressure daily variability, based on 30 years of data and after substracting the annual cycle. a) LMD-GCM for the NH, b) NCEP reanalysis for the NH, c) LMD-GCM for the SH, and d) NCEP reanalysis for the SH. Contour interval 1hPa.

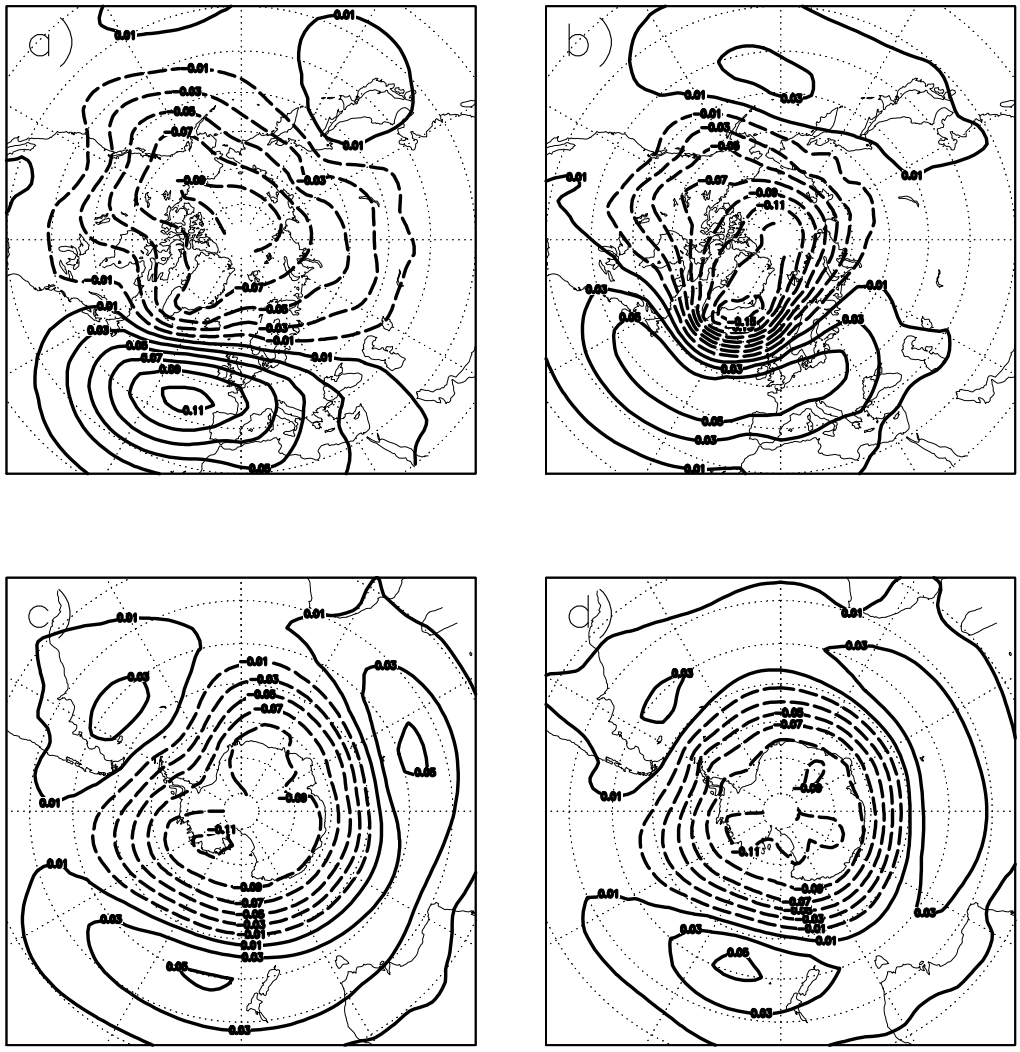

Figure 2. Leading EOF of Hemispheric daily variability, based on 30 years of data and after substracting the annual cycle. a) LMD-GCM for the NH, b) NCEP reanalysis for the NH, c) LMD-GCM for the SH, and d) NCEP reanalysis for the SH. Contour interval 0.02, and negative values are dashed.

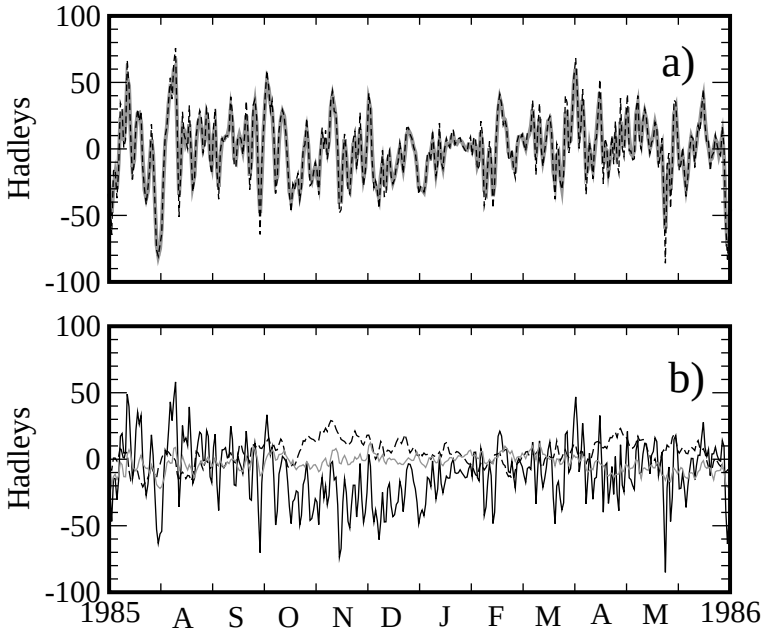

Figure 3. Model atmospheric angular momentum balance and torques over one year. a) Global AAM tendency (heavy grey) and total torque (dashed). b) Mountain torque (black), frictional torque (dashed), and subgrid scale orography torque (grey).

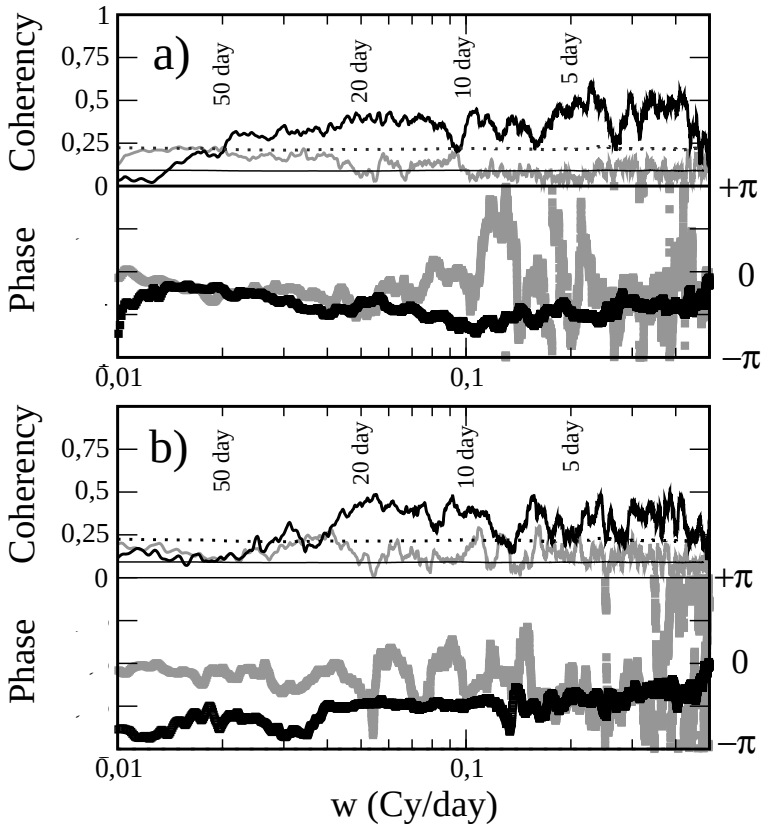

Figure 4. Cross spectral analysis between the mountain torque and the AO (black) and the AAO (grey). a) Results from the model; b) Result from the reanalysis. The upper panels in a) and b) present the coherencies, the lower panel are for the phases. In both a) and b) the coherencies and phases are deduced from the cross periodigrams and the periodigrams of the series, each of them smoothed by a 100 points 10%-cos window. In the frequency domain, this yields to a resolution of 10^{-2}Cy/day. For the coherencies, the 1% confidence level is also displayed. It is evaluated via a Monte Carlo procedure, which uses an ensemble of 100 pairs of independent red-noise series whose variance and lag 1 correlations correspond to those of T_M and of the PC 1s.

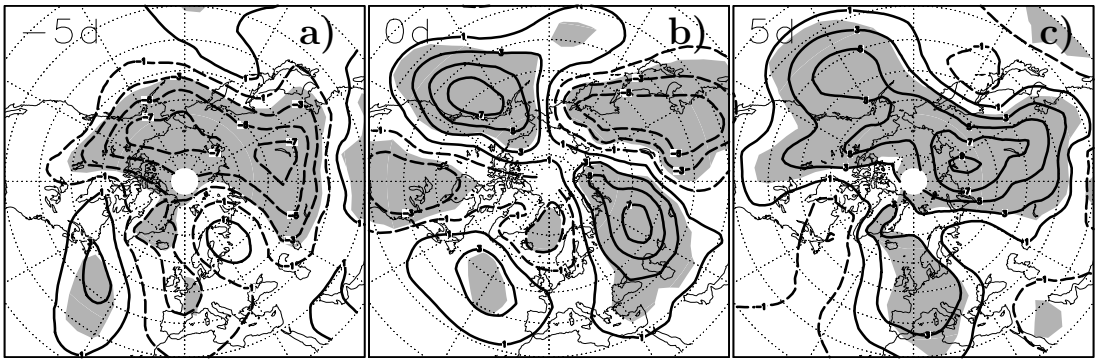

Figure 5. Composite of the IS sea-level pressure fields keyed to minus the IS mountain torque. (a) -5 day lag; (b) 0 day lag; and (c) 5 day lag. Contour interval: 2hPa; positive values, heavy solid; negative values, heavy dashed. 1% confidence shaded. The days for each composite cycle are counted from the local extremum of the IS T_M.

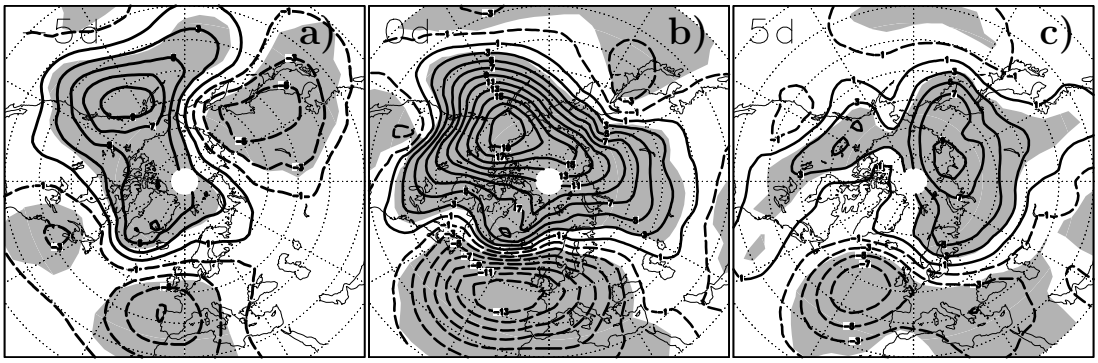

Figure 6. Same as Fig. 5 but for composites keyed to minus the IS AO.

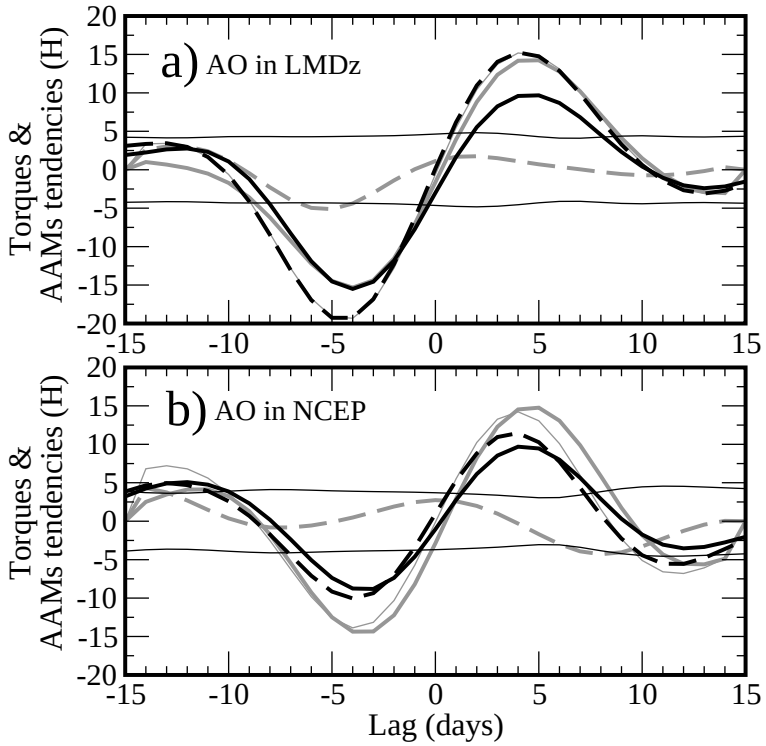

Figure 7. Composites of different terms in the AAM budget, keyed to minus the IS-AO: a) LMDz model, b) NCEP reanalysis. IS M_Ω tendency (thick grey); IS M_R tendency (thick grey dashed); IS total AAM (M) tendency (thin grey); IS T_M (thick black); and IS total torque T (thick black dashed). The thin black lines are 1% confidence levels for the IS T_M, evaluated with a student test with N degrees of freedom, N being the number of dates selected to build the composites..

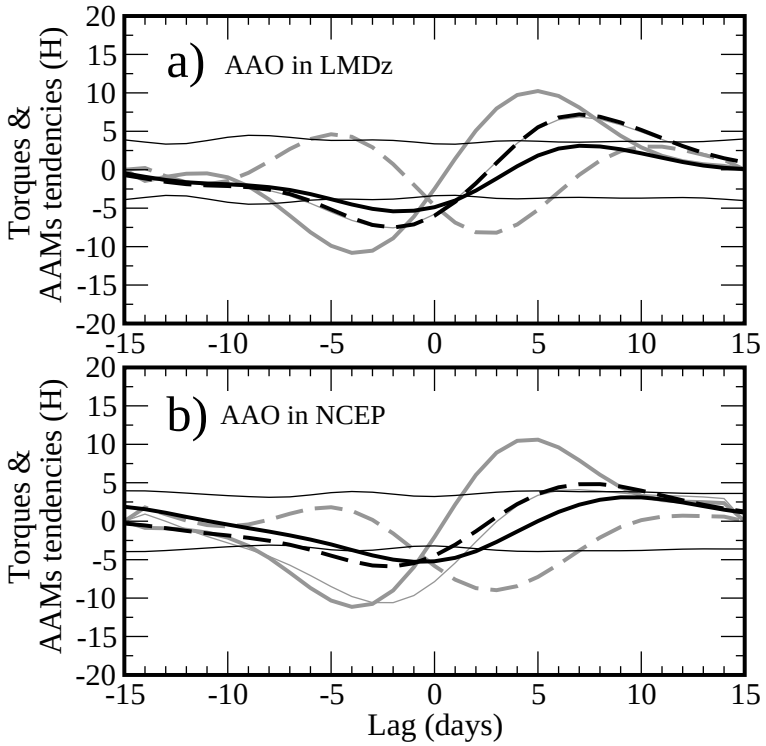

Figure 8. Same as Fig. 7 but for the Antarctic Oscillation.